International Nonwoven
Technical Conference
Houston, TX, USA, 2006.

Computer Models of Nonwoven Geometry and Filtration Simulation

Andreas Wiegmann, PhD, Dr. Stefan Rief and Dr. Arnulf Latz
Fraunhofer Institut für Techno- und Wirtschaftsmathematik,
Kaiserslautern, Germany

Abstract

A geometric model for the 3 dimensional structure of nonwoven was developed. It contains the porosity, fiber diameters and fiber anisotropy as parameters, and results in complex realizations of the media. Due to the use of a random number generator, no two realizations look alike albeit they all satisfy the requirements for porosity, fiber diameter distribution and fiber anisotropy within a prescribed tolerance. This is very similar to real nonwoven, where no two small samples ever look exactly the same.

In these structures, the fluid flow and particle deposition are simulated. Initial pressure drop, filter efficiency and filter lifetime are quantities that are computed based on the nonwoven, the mean flow velocity and the particle size distribution. Additionally, electric charges, adhesion forces and in case of very small particles, diffusion may play a role.

With this simulation chain from nonwoven geometry to filtration properties, ultimately the virtual material design of nonwoven will become feasible: For a given filtration application, an optimal, possibly graded nonwoven is sought by an automated computer simulation that finds the best nonwoven parameters. Of course, also other than filtration properties can be simulated, current interests lie in deformations, acoustic absorption and effective strength.

Keywords: nonwoven model, nonwoven property simulation, particle filtration simulation.

Introduction

Computer simulations have the potential to revolutionize the development process in the nonwoven industry. The great advantages of manmade fibers are their designability and uniformity. Based on these properties, nonwoven parameters such as porosity, fiber thickness distribution, fiber orientation and porosity gradients are to a large extent at the command of the experienced nonwoven manufacturer. The problem is usually the cost of trying out new parameter sets. Lab scale production often does not completely agree with production scale nonwoven, and stopping the production lines for parameter studies is very costly. Computer simulations can reduce the number of trial runs of producing new material prototypes significantly. They help understanding the production processes as well as the functionality of the nonwoven and may point out trends or improvements that would be costly to find using traditional methods. Thus, much work has gone into understanding nonwoven and building

nonwoven models [1, 2, 3, 4, 5]. Both porosity and fiber thickness or fiber shapes are comparatively easy to determine. Much harder is the estimation of fiber orientation. In [2], a simple nonwoven model is developed based on the assumptions that the portion of the nonwoven that can be represented in the computer memory is small compared to fiber length and fiber crimp. Thus, fibers are viewed as infinitely long lines, with appropriate thickening and orientation. Hollow fibers or noncircular cross section shapes are easily introduced by simply changing the cross section shape while keeping the area constant. The porosity is governed by the number of fibers, and in the simplest case, fibers are allowed to overlap, possibly modeling a thermal bonding process. To reproduce existing media, the grammage and specific weight of the fiber material can be used to infer the porosity from the thickness of the nonwoven. Manufacturers usually know the types of fibers they use, so the only difficulty lies in establishing the orientation. In [2], a 1-parameter model for the anisotropy is developed that generates anisotropic virtual nonwoven that are isotropic in the plane of the media, but have a controlled anisotropy in the through direction of the media. Figure 3 shows a three-dimensional view and Figure 4 shows cross section views of a highly anisotropic nonwoven with 90% porosity, circular fibers of 5.4 and 3.0 dtex, resolved at 2.8µm per voxel.
Based on this nonwoven model, the compression of the media and addition of binder to the model were introduced in [6]. There, the same nonwoven models and one-phase flow simulations that are also used for the filtration simulations are used in modeling the gas diffusion layer (GDL) in fuel cells. In earlier and ongoing work, the acoustic absorption properties of nonwoven were studied via simulation. Figure 5 shows cross section models of the same media as in Figure 4, but compressed by 20% and with binder added. The methods to validate the models include visual inspection, i.e. comparison with microscopy, comparison of geometric measures such as chord length distributions [1] or pore size distribution (c.f. Figure 6), but ultimately agreement and prediction of material properties such as flow resistivity, relative diffusivity or thermal conductivity [7]. Based on the flow computations in the nonwoven model [8], one can predict the filtration properties of nonwoven filter media [10, 11, 12]. Ultimately, when agreement of simulation results is achieved for tomographic images and computer models, the quest for improved virtual nonwoven can begin. Once they are found, the manufacturer is challenged with actually producing nonwoven with the properties found to be optimal by the simulations.

Some theory of filtration simulation

The Stokes equations describe the motion of a fluid for very slow regimes that occur in many filtration applications. The pressure difference, together with the media model, provides the needed boundary conditions. The media is viewed to consist of a collection of empty and solid voxels, and the flow can only occur in the empty space. On the surfaces of the solid voxels, the velocity is prescribed to be zero, while the pressure difference is converted into a driving force for the flow equations. Figure 1 shows the Navier-Stokes-Brinkmann equations, the most complete formulation of steady fluid flow used in our computations: they include the nonlinear inertia term and a Darcy-type permeability κ that is capable of modeling effects that are not resolved by the full or empty voxels, namely by permeable voxels. Figure 7 a) shows the pressure distribution and Figure 7 b) shows the magnitude of the velocity computed by the Stokes equations for air flowing through the layer that was shown in Figure 4 a). The flow is considered stationary, that means it does not change with time, and computed by an Eulerian model, that means that for every computational cell a value for the pressure and three values for the velocity are found.

$$
\begin{aligned}
-\mu\Delta\vec{u} + \nabla\vec{u}\cdot\vec{u} + \kappa^{-1}\vec{u} + \nabla p &= \vec{\mathrm{f}} \text{ (momentum balance)} \\
\nabla\cdot\vec{u} &= 0 \text{ (mass conservation)} \\
\vec{u} &= 0 \text{ on } \Gamma \text{ (no-slip on fiber surfaces)}
\end{aligned}
$$

$\vec{\mathrm{f}} = (0,0,f)$: force in flow(z)-direction,
κ : porous voxel permeability,
$\vec{u}$: velocity,
μ : fluid viscosity,
p : pressure and
Γ : surfaces of fibers or deposited particles.

Figure 1. *Navier-Stokes-Brinkmann equations and notation.*

Based on this computed flow field, the motion and deposition of spherical particles of various sizes is computed by a Lagrangian formulation for the particle motion. That means that a particle can move freely through the pores according to its inertia, the friction with the air, possibly electric charges, and due to diffusion, the random motion also called Brownian motion that affects mostly very small particles. The velocities and electric forces are interpolated from the flow grid to the precise position of the particle. Figure 2 shows the equations for the particle motion. The three terms influencing the particle acceleration dv/dt are the friction with the fluid, the electric field, and diffusion.

$$
\begin{aligned}
\frac{d\vec{v}}{dt} &= -\gamma\times(\vec{v}(\vec{x}) - \vec{v}_\circ(\vec{x})) + \frac{Q\vec{E}_\circ(\vec{x})}{m} + \sigma\times\frac{d\vec{W}(t)}{dt} \\
\frac{d\vec{x}}{dt} &= \vec{v} \\
\gamma &= 6\pi\rho\mu\frac{R}{m} \\
\sigma^2 &= \frac{2k_B T\gamma}{m} \\
\left\langle dW_i(t), dW_j(t)\right\rangle &= \delta_{ij}dt
\end{aligned}
$$

t: time
$\vec{x}$: particle position
$\vec{v}$: particle velocity
R: particle radius
m: particle mass
Q: particle charge
T: ambient temperature
k_B: Boltzmann constant
$d\vec{W}(t)$: 3d probability (Wiener) measure
$\vec{E}_\circ$: electric field
$\vec{v}_\circ$: fluid velocity
ρ: fluid density
μ: fluid viscosity

Figure 2. Lagrangian description of particle motion.

Besides the flow field, electric field, and particle motion, collisions of the particles with the fibers are treated. In the simplest model, a particle is thought as captured as soon as it touches a fiber. By analyzing the number of captured particles of a certain size against the total number of particles of this size, a filter efficiency diagram can be simulated. Figure 8 a) shows particles in

motion through the filter media and Figure 8 b) shows a filter efficiency diagram for the same data.
By modifying the nonwoven geometry by the deposited particles and re-computing the flow field (now with no-slip boundary conditions also on the surfaces of the deposited particles), this procedure can be iterated and the clogging of the filter media as more and more dust is deposited can be simulated.
By changing the parameters of the simulation such as fluid velocity, fluid viscosity, particle size distribution, and particle – fiber adhesion as well as the nonwoven parameters, a wide range of fluid – particle and gas – particle separation applications are in the range of the simulation. As examples, the group currently treats oil and blood, as well of air as fluid and deals with particles representing standard test dusts such as SAE fine, blood cells or soot.

Results

With careful modeling of the nonwoven, test dust, flow regime, electric field and particle – fiber adhesion, it is possible to achieve good agreements between the simulation and measurements. We illustrate this by two data sets. The first example in Figure 9 shows the average over ten measurements against 3 individual simulation runs. The averaged measurement yields the smoother curve, but this is due to the averaging. The individual simulation runs produce even non-monotone curves, but averaging them would yield results very close to the measurements. The second example in Figure 10 shows the pressure drop evolution with time. Here, a peculiar shape of the curve can be seen due to an initial phase of depth filtration with some interesting variation in slope followed by a phase with constant slope where cake filtration occurs. Also this behavior of the pressure drop can be observed in reality. Both examples give an impression that it is possible to capture the behavior of real filtration processes with the simulations.

Conclusions

The described methodology of modeling nonwoven media together with the simulation of fluid flow and particle tracking and particle depositing provides deep insights into the filtration processes in complex filter media. Nonwoven geometries, pressure distributions, local flow velocities, media clogging, filter efficiencies and filter lifetime including pressure drop evolution and filter efficiency over time are visualized and evaluated. Comparisons with measurements on real media show that the simulations are capable of producing many real effects and have the potential to provide valuable insights on how to design new filter media for modern filtration applications. Many of the simulations can be carried out on top of the line PCs and can be tried by interested parties by downloading the Software for evaluation purposes from http://www.geodict.com.

References

[1] J. Ohser u. F. Mücklich, *Statistical Analysis of Microstructures in Materials Science*, John Wiley & Sons (2000).

[2] K. Schladitz, S. Peters, D. Reinel-Bitzer, A. Wiegmann, J. Ohser, *Design of acoustic trim based on geometric modeling and flow simulation for nonwoven*, ITWM Technical Report Nr. 72, January 2005. Accepted in Computational Material Science.

[3] H. Yang and W.B.Lindquist. *A Geometric Analysis on 3D Fiber Networks from High Resolution Images.* International Nonwovens Technical Conference, Dallas, 2000.

[4] B. Pourdeyhimi, *Assessing Fiber Orientation in Nonwoven Fabrics*, INDA Journal of Nonwovens Research, 5, (3), 29-36, (1993).

[5] B. Pourdeyhimi and H. S. Kim, *Measurement of Fiber Orientation in Nonwovens: Hough Transform*, Textile Research Journal, 72 (9), 803-809 (2002)

[6] V. Schulz, J. Becker, A. Wiegmann, P. Mukherjee and C.-Y. Wang: *Modelling of Two-phase Behaviour in the Gas Diffusion Medium of Polymer Electrolyte Fuel cells via Full Morphology Approach*, submitted to J. App. Phys, 2006.

[7] V. Schulz, D. Kehrwald, A. Wiegmann, K. Steiner. *Flow, heat conductivity, and gas diffusion in partly saturated microstructures*, NAFEMS Seminar: "Simulation of Complex Flows (CFD)", Niedernhausen/Wiesbaden, April 2005.

[8] A. Wiegmann, *A fast fictitious force 3d Stokes solver*, in preparation, 2006.

[9] R.C. Brown, *Air Filtration, an Integrated Approach to the Theory and Application of Fibrous Filters*, Pergamon Press, Oxford (1993).

[10] A. Latz and A. Wiegmann, *Simulation of fluid particle separation in realistic three dimensional fiber structures*, Filtech Europa, Düsseldorf, October 2003.

[11] A. Wiegmann, S. Rief and A. Latz, *Virtual Material Design and Air Filtration Simulation Techniques inside GeoDict and FilterDict*, American Filtration and Separation Society annual meeting, Atlanta, 2005.

[12] S. Rief, A. Latz and A. Wiegmann, *Research Note: Computer simulation of Air Filtration including electric surface charges in three-dimensional fibrous micro structures*, Filtration, Vol. 6 No. 2, 2006.

Figure 3. *3-dimensional view of a 200³ realization of a nonwoven with two different fiber types. 5.4 dtex fibers are shown orange and 3 dtex fibers are shown in red. The anisotropic fiber orientation is "almost" parallel to the x-y plane.*

Figure 4. *a) X cross section view of a 500³ voxel virtual nonwoven media model with 90 % porosity. b) Z cross section view of the same, highly anisotropic media. The Y-cross section view looks similar to the X cross section view.*

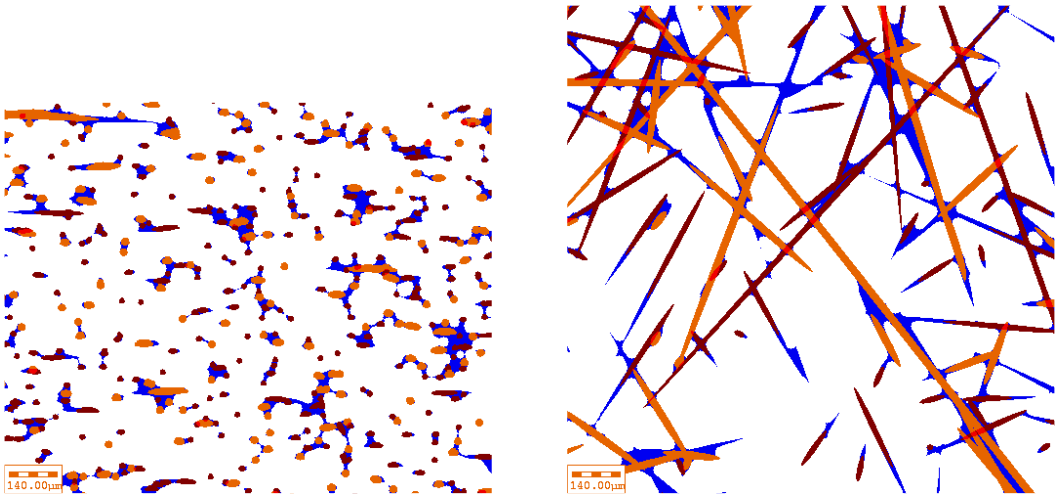

Figure 5. *a) X cross section view as in Figure 3a) but compressed by 20% and with binder in blue. b) Z cross section view as in Figure 3b) with binder in blue.*

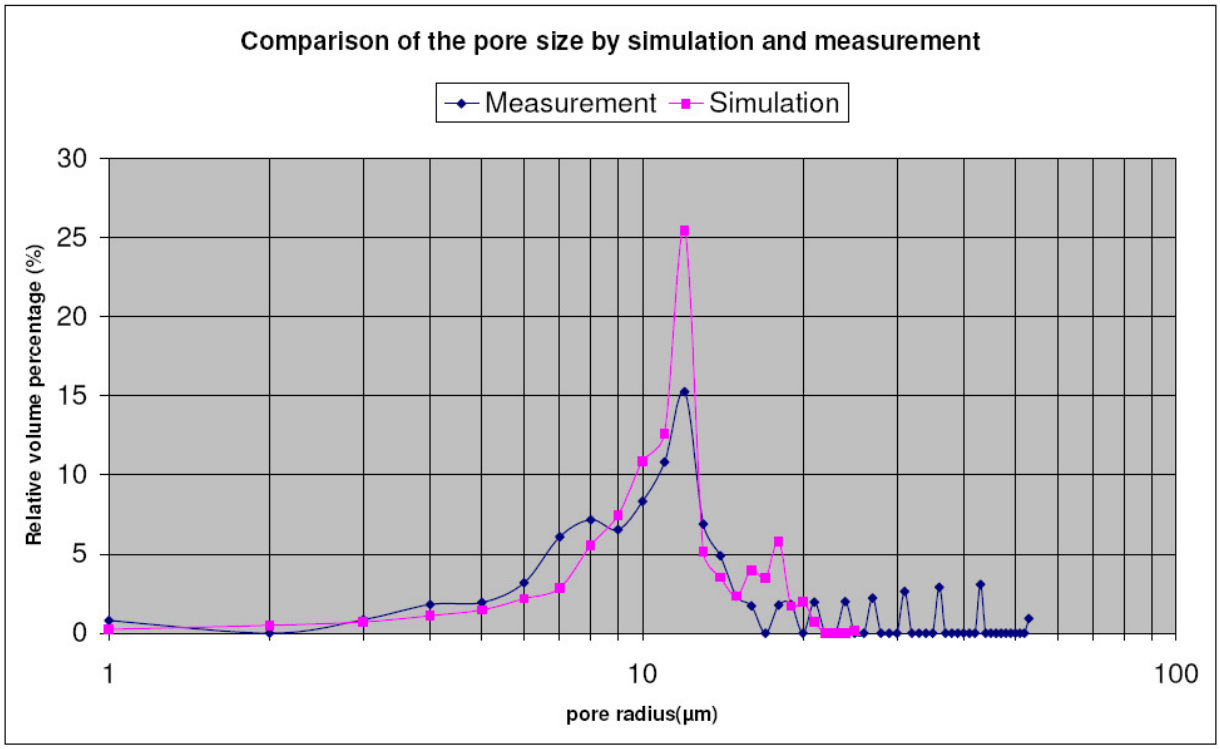

Figure 6. *Pore size measurements by the mercury intrusion method in dark blue vs. the computed pore size distribution of a media model of the same material in pink. The media was described by a frequency distribution of 20 fiber types. The discrepancy for large pore sizes bigger than 30 microns is still under investigation, and is currently considered an artefact of the experimental method.*

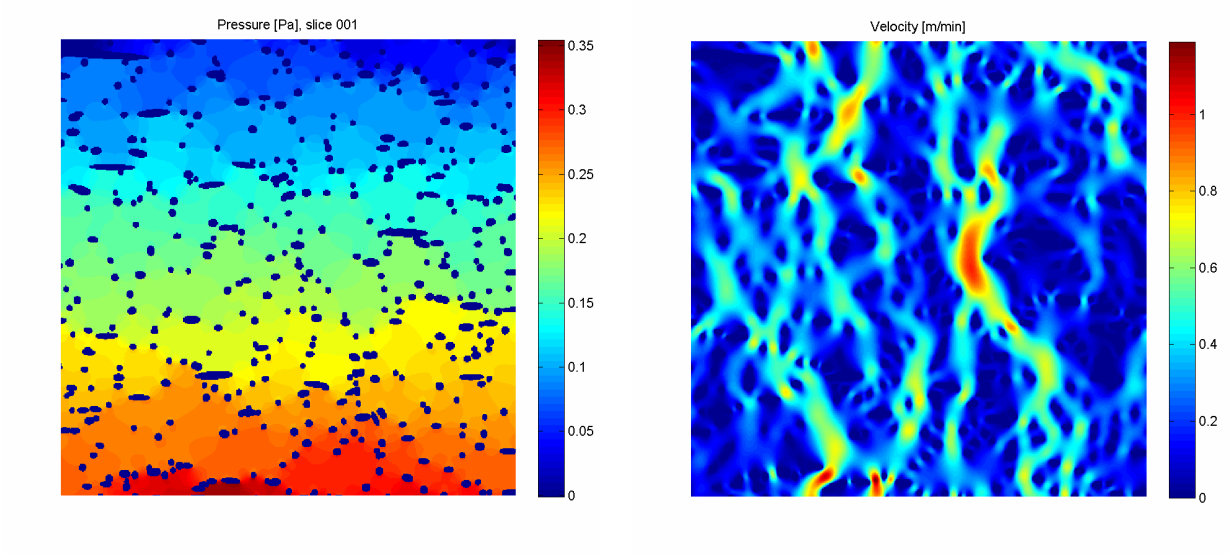

Figure 7. *X cross section view of a) Pressure distribution and b) magnitude of velocity distribution in the media from Figure 3. The fibers are shown as darkest blue while the lighter colors indicate magnitude of pressure and velocity, respectively. The flow direction is from bottom to top.*

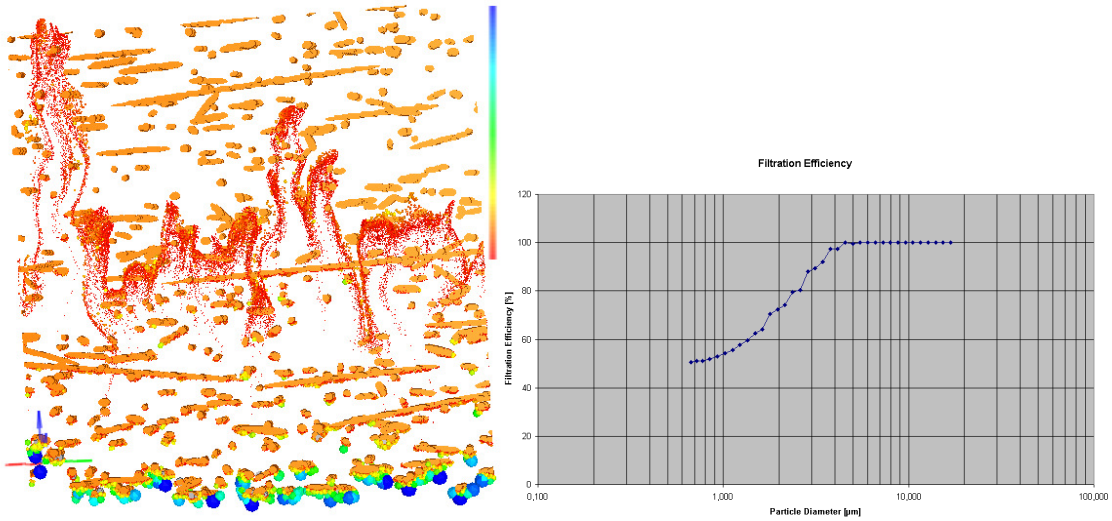

Figure 8. *a) Visualization of the particles in motion. In this setup, the large particles in blue, yellow and green are caught already on the surface of the media and filtered out. Only the smallest particles in red penetrate the media, the snapshot shows a visualization as if all of the started at the same time. Then, their position also gives an impression of the local flow velocities. B) Filter efficiency chart for this example. The largest particles are all filtered, while for smaller particles a smooth curve can be seen. Conceivably, the filter efficiency would go up again for even smaller particles, due to the kicking in of the diffusion effect.*

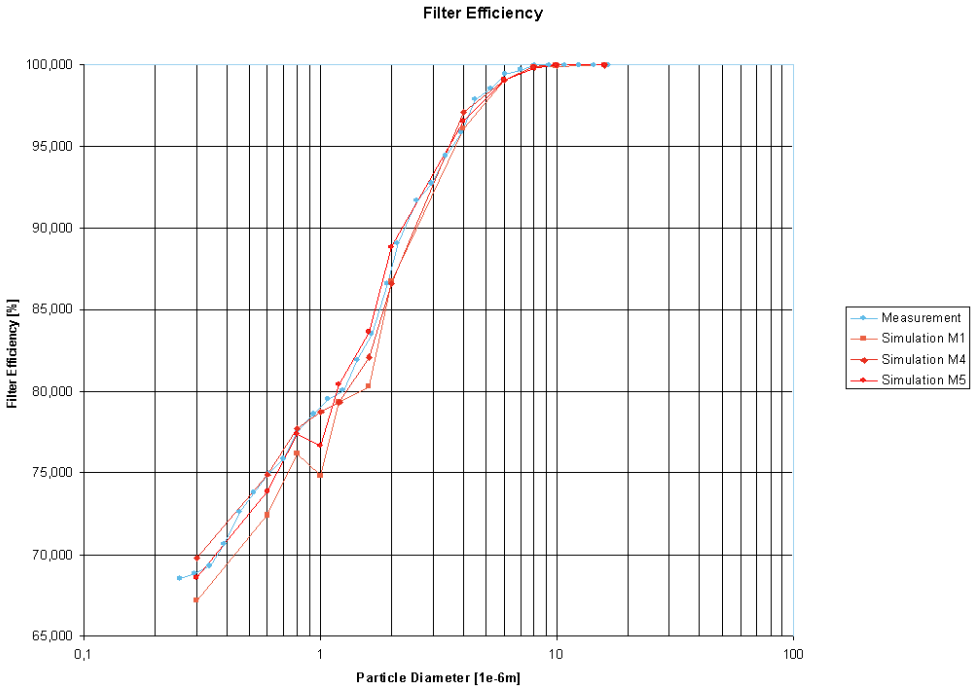

Figure 9. *Filter efficiency simulation and measurements. Three different realizations of the same nonwoven media were used in flow and filter efficiency simulations and are shown in orange . They are compared against an average over 10 measurements, shown in blue.*

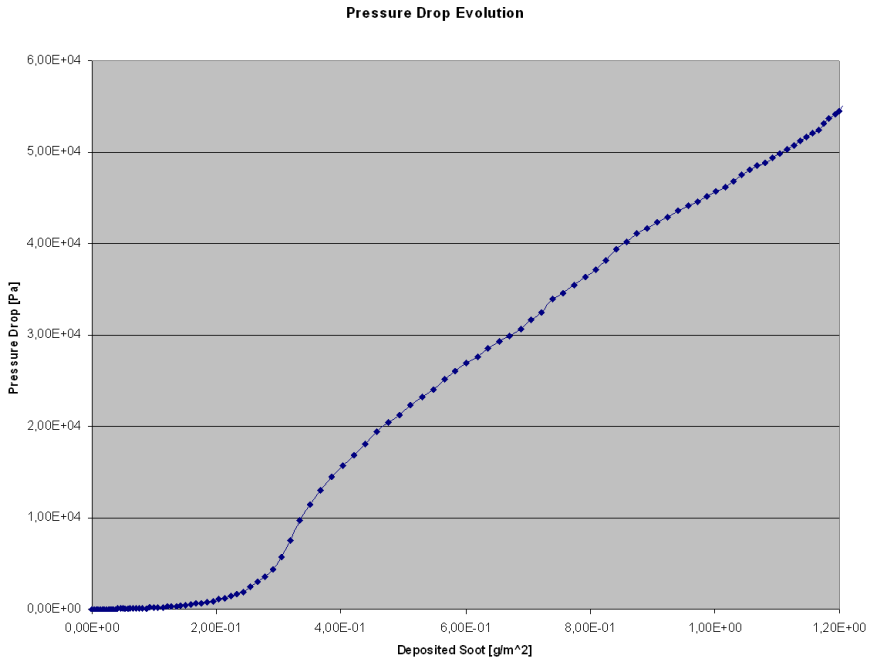

Figure 10. *Evolution of pressure drop over deposited soot. The curve shows the typical behavior that is also measured, with a reflection point (change in the sign of curvature) near 3 g/m², where the type of filtration mechanism switches from depth filtration to cake filtration. (Example of a filtration in metal rather than textile fibers)*